

1 **Microbial iron uptake in the naturally fertilized waters in the vicinity of Kerguelen**  
2 **Islands: phytoplankton-bacteria interactions**

3 **M. Fourquez<sup>1,2,3\*</sup>, I. Obernosterer<sup>2,3</sup>, D. M Davies<sup>4,5</sup>, T. W. Trull<sup>4,5</sup>, and S. Blain<sup>2,3</sup>**

4 <sup>1</sup> Institute for Marine and Antarctic Studies, University of Tasmania, Hobart 7001, Australia

5 <sup>2</sup> Sorbonne Universités, UPMC Univ Paris 06, UMR 7621, Laboratoire d'Océanographie  
6 Microbienne, Observatoire Océanologique, F-66650 Banyuls/mer, France

7 <sup>3</sup> CNRS, UMR 7621, Laboratoire d'Océanographie  
8 Microbienne, Observatoire Océanologique, F-66650 Banyuls/mer, France

9 <sup>4</sup> CSIRO Oceans and Climate Flagship, Hobart 7001, Australia

10 <sup>5</sup> Antarctic Climate and Ecosystems Cooperative Research Centre, Hobart 7001, Australia

11 \* Corresponding Author

12 Key words: Iron, phytoplankton, heterotrophic bacteria, natural iron fertilization, Southern  
13 Ocean, competition

14 Running title: Microbial iron uptake

15 **ABSTRACT**

16 Iron (Fe) uptake by the microbial community and the contribution of three different  
17 size-fractions was determined during spring phytoplankton blooms in the naturally Fe  
18 fertilized area off Kerguelen Islands (KEOPS2). Total Fe uptake in surface waters was on  
19 average  $34 \pm 6$  pmol Fe L<sup>-1</sup> d<sup>-1</sup>, and microplankton (>25µm size-fraction; 40-69%) and pico-  
20 nanoplankton (0.8-25 µm size-fraction; 29-59%) were the main contributors. The contribution  
21 of heterotrophic bacteria (0.2-0.8 µm size-fraction) to total Fe uptake was low at all stations  
22 (1-2%). Iron uptake rates normalized to carbon biomass were highest for pico-nanoplankton  
23 above the Kerguelen plateau and for microplankton in the downstream plume. We also  
24 investigated the potential competition between heterotrophic bacteria and phytoplankton for  
25 the access to Fe. Bacterial Fe uptake rates normalized to carbon biomass were highest in  
26 incubations with bacteria alone, and dropped in incubations containing other components of  
27 the microbial community. Interestingly, the decrease in bacterial Fe uptake rate (up to 26-  
28 fold) was most pronounced in incubations containing pico-nanoplankton and bacteria, while  
29 the bacterial Fe uptake was only reduced by 2- to 8- fold in incubations containing the whole  
30 community (bacteria + pico-nanoplankton + microplankton). In Fe-fertilized waters, the  
31 bacterial Fe uptake rates normalized to carbon biomass were positively correlated with  
32 primary production. Taken together, these results suggest that heterotrophic bacteria are  
33 outcompeted by small sized phytoplankton cells for the access to Fe during the spring bloom  
34 development, most likely due to the limitation by organic matter. We conclude that the Fe and  
35 carbon cycles are tightly coupled and driven by a complex interplay of competition and  
36 synergy between different members of the microbial community.

## 37 **1. INTRODUCTION**

38           Microorganisms in the ocean are characterized by widespread distributions, large  
39 abundances and high metabolic rate activities. Consequently they play a pivotal role in  
40 biogeochemical cycles of many elements (Arrigo, 2005; Madsen, 2011). Following the  
41 pioneering work of Martin (1990), a major achievement in the past decades has been the  
42 discovery of the tight, but complex link between the carbon and iron (Fe) biogeochemical  
43 cycles in the ocean. Thus, it is not surprising that microorganisms play a crucial role in the  
44 functioning and the coupling of both cycles. Autotrophs are a net carbon dioxide (CO<sub>2</sub>) sink  
45 and heterotrophs are a net CO<sub>2</sub> source, but both require Fe to process carbon. Therefore, the  
46 balance between autotrophy and heterotrophy and ultimately the air-sea CO<sub>2</sub> flux should be  
47 influenced by Fe availability for microorganisms. This issue is definitively critical in  
48 environments receiving low Fe supply, like the high nutrient low chlorophyll regions  
49 (HNLC).

50           The role of heterotrophic bacteria has been far less studied than that of phytoplankton.  
51 However, essential data for the understanding of the responses of heterotrophic bacteria to Fe  
52 limitation have already been collected. Iron uptake rates, Fe cellular contents and Fe/carbon  
53 ratios were determined in various environments (Tortell et al., 1996; Maldonado et al., 2001;  
54 Sarthou et al., 2008). Culture experiments (Granger and Price, 1999, Fourquez et al., 2014)  
55 have elucidated some of the metabolic pathways affected by Fe limitation which may explain  
56 the changes observed in Fe-limited heterotrophic cells or communities. Additionally, the  
57 obligate requirement of Fe for heterotrophic bacteria and phytoplankton suggests that both  
58 organisms are competing for Fe acquisition. The competition between phytoplankton and  
59 bacteria was addressed experimentally (Mills et al., 2008) and conceptually (Litchman et al.,  
60 2004) for the access to nitrogen and phosphorus, but this issue has been rarely studied in the  
61 case of Fe (Boyd et al., 2012). Beside this possible pure competition, both autotrophic and

62 heterotrophic microorganisms could also benefit from each other. Phytoplankton are a source  
63 of carbon for heterotrophic bacteria and the production of ligands by these latter could make  
64 Fe available for other microorganisms (Amin et al., 2009; Hassler et al., 2011a, 2011b). The  
65 aim of our study was to investigate further the complex interactions between heterotrophic  
66 bacteria and phytoplankton, with respect to the carbon and Fe cycling.

67         The Southern Ocean is the largest HNLC region in the world ocean. However, at  
68 several places, natural Fe fertilization sustains massive blooms (Blain et al., 2007; Nielsdóttir  
69 et al., 2012; Pollard et al., 2009). These natural fertilized regions are exceptional laboratories  
70 to study interactions between the Fe and carbon cycling and the role played by  
71 microorganisms. The bloom located above the Kerguelen Plateau was investigated in detail  
72 during KEOPS1 (Kerguelen Ocean and Plateau compared Study) (Jan-Feb 2005). KEOPS2  
73 (Oct-Nov 2011) extended this study to early stages of the bloom and to new investigations in  
74 the blooms downstream the island. During KEOPS2 we have determined the Fe uptake of the  
75 bulk microbial community and of different size-fractions at stations characterized by a wide  
76 range of responses to Fe fertilization. We have also conducted an incubation experiments to  
77 specifically study the competition between heterotrophic bacteria and phytoplankton.

## 78 **2. MATERIALS AND METHODS**

### 79 **2.1. Site description**

80         This study was carried out as part of the KEOPS2 expedition that took place from 9  
81 October to 29 November 2011, in the Indian sector of the Southern Ocean in the vicinity of  
82 the Kerguelen archipelago. For the present study 8 stations were sampled (Fig. 1). Station R-2  
83 is the reference station located outside the bloom, west of Kerguelen Island (Fig. 1). The  
84 stations E were located in a complex meander south of the Polar Front and sampled in a quasi-  
85 Lagrangian manner (d'Ovidio et al., 2015). An animation is given in supplement material that

86 shows the development of the bloom over the period of the cruise and position of the stations  
87 at the time of sampling (Supplement 1).

## 88 **2.2. Sampling and manipulation under trace metal clean conditions**

89 Seawater samples were collected with 10-Liters Niskin 1010X-bottles set up on the  
90 autonomous Trace Metal Rosette 1018 especially adapted for trace metal work (General  
91 Oceanics Inc., USA; Bowie et al., 2014). Each Niskin bottle was acid-washed (2% HCl) and  
92 rinsed with milli-Q water before the rosette was deployed. All metal springs are Teflon coated  
93 and the crimps are made of aluminium. All samples were carefully manipulated in a clean  
94 container under a laminar flow hood (ISO class 5). Within less than 2 hours after sample  
95 collection, the seawater was dispersed into 500 mL acid-washed polycarbonate (PC) bottles  
96 and the incubations performed as described below. The PC bottles were acid-washed (10%  
97 HCl suprapur, Merck) three times, followed by three rinses with milli-Q-water and they were  
98 subsequently sterilized by microwaves (5 minutes, 750W). The PC bottles were dried and  
99 stored under a laminar flow hood before being used. For the incubation experiments described  
100 below, seawater was collected in the surface mixed layer at one depth, and incubated at  
101 different levels of surface photosynthetically active radiation (PAR). Characteristics of the  
102 stations are given in Table 1.

## 103 **2.3. Iron uptake experiments**

104 Three types of incubation experiments were performed (Fig. 2). In one set of  
105 experiments, 300 mL of unfiltered seawater were amended with Fe as  $^{55}\text{FeCl}_3$  (0.2 nM final  
106 concentration of  $^{55}\text{Fe}$ , specific activity  $1.83 \times 10^3 \text{ Ci mol}^{-1}$ , Perkin Elmer), incubated for 24h  
107 at 75%, 25% and 1% surface PAR, and then sequentially filtered through 0.8  $\mu\text{m}$  and 0.2  $\mu\text{m}$   
108 pore size nitrocellulose filters (47mm diameter, Nuclepore)(Fig. 2a). These incubations,  
109 performed at station A3-2, E-4E and E-5, provided measurements of the Fe uptake of the bulk

110 community based on the sum of the radioactivity measured on the 0.8 $\mu$ m and 0.2 $\mu$ m filters.  
111 The uptake of Fe by heterotrophic bacteria incubated with the whole community (bacteria +  
112 pico-nanoplankton + microplankton) was also determined from these incubations. In a second  
113 set of experiments, seawater (300 mL) was pre-filtered through a 25  $\mu$ m mesh before 0.2 nM  
114  $^{55}\text{Fe}$  (final concentration) was added. This porosity was chosen to exclude microplankton by  
115 retaining them on the 25  $\mu$ m mesh. Following incubation at 75, 45, 25, 16, 4, and 1% of  
116 surface PAR, the seawater was sequentially filtered through 0.8 $\mu$ m and 0.2  $\mu$ m filters (Fig.  
117 2b). The uptake of Fe by pico-nanoplankton (0.8-25  $\mu$ m), and that of heterotrophic bacteria  
118 (0.2-0.8  $\mu$ m) in the presence of pico-nanoplankton only was derived from these incubations.  
119 At the stations where these two types of experiments were performed concurrently (station  
120 A3-2, E-4E and E-5), the Fe uptake by microplankton was obtained by the difference between  
121 the bulk Fe uptake (Fig. 2a) and the sum of the Fe uptake by pico-nanoplankton and  
122 heterotrophic bacteria (Fig. 2b). In a third set of experiments, 300 mL seawater was 0.8  $\mu$ m  
123 pre-filtered prior to the addition of 0.2 nM  $^{55}\text{Fe}$  (final concentration), to exclude both  
124 microplankton and pico-nanoplankton from the incubation. Following the 24h incubation at  
125 1% PAR level, the seawater was filtered on a 0.2  $\mu$ m filter (Fig. 2c). Based on this type of  
126 incubation, we determined the Fe uptake by heterotrophic bacteria in incubations with  
127 bacteria alone. This experiment was performed at stations A3-2, E-4E, E-5, E-4W and R-2.

128 For all the incubations, bottles were maintained at *in situ* surface temperature (Table 1)  
129 in on-deck incubators supplied continuously with surface seawater. The incubators were  
130 equipped with a combination of Nickel screens (LEE Filters, UK) simulating light intensities  
131 from 75% to 1%. Incubations were conducted from dawn to dawn.

132 Additionally, to determine if a steady state has been achieved after 24 hours of  
133 incubation time we performed a separate set of experiments where Fe uptake by bacteria and  
134 bacterial cell abundance was followed over 24, 72, 96h and one week incubation time. Due to

135 the low bacterial Fe uptake rates determined over 24h, we did not perform any time series  
136 over shorter incubation times. Our results are therefore based on the assumption of linearity in  
137 bacterial Fe uptakes rates over the 24h incubation period.

#### 138 **2.4. Determination of intracellular $^{55}\text{Fe}$**

139 A first step for the assessment of the  $^{55}\text{Fe}$  uptake was the removal of  $^{55}\text{Fe}$  not  
140 incorporated by cells, using a washing solution. Following filtration, the filters were washed  
141 with 6 mL of Ti-citrate-EDTA solution (Hudson and Morel, 1989; Tang and Morel, 2006) for  
142 2 minutes and subsequently rinsed 3 times with 5 mL of 0.2  $\mu\text{m}$  filtered seawater for 1 minute  
143 (Fourquez et al., 2012). The filters were placed into plastic vials and 10 mL of the scintillation  
144 cocktail Filtercount (Perkin Elmer) were added. Vials were agitated for 24 hours before the  
145 radioactivity was counted with the Tricarb® scintillation counter. Total radioactivity on filter  
146 after correction for background represents intracellular  $^{55}\text{Fe}$ . For each station, controls were  
147 obtained with 300 mL of microwave-sterilized seawater (750 W for 5 minutes repeated 3  
148 times) incubated with the same amount of  $^{55}\text{Fe}$  and treated in the same way as the live  
149 treatments. The radioactivity determined on these filters was considered as background and it  
150 is based on the amount of  $^{55}\text{Fe}$  absorbed, but not incorporated by cells. Abiotic adsorption of  
151  $^{55}\text{Fe}$  onto cells could be influenced by microwave irradiation if cell structures are altered by  
152 the treatment. For technical reasons, we could not use formalin to fix the cells at each station,  
153 but we performed a series of tests to compare fixation by formalin and by microwave. The  
154 background radioactivity of the formalin-killed seawater was similar to that of the  
155 microwave-sterilized seawater, validating our control. We performed one control per station  
156 maintained for 24h at 75% PAR in the on-deck incubator. The radioactivity measured on the  
157 control filters was subtracted from the respective live treatments in all experiments.

158 To determine the most appropriate concentration of the radioisotope to be added,  
 159 different amounts of  $^{55}\text{Fe}$  were tested: 0.2, 0.4, 1 and 2 nM of unchelated  $^{55}\text{Fe}$  (as  $^{55}\text{FeCl}_3$ ,  
 160 final concentrations of  $^{55}\text{Fe}$ ). We determined that the concentration of 0.2 nM  $^{55}\text{Fe}$  was the  
 161 most appropriate as it minimizes changes in dissolved Fe (DFe) and it still allows detection of  
 162 the incorporated radioactivity by scintillation counting (for 300 mL of seawater). We also  
 163 observed that adding more than 0.8 nM of  $^{55}\text{Fe}$  (final concentration) stimulates the Fe uptake  
 164 by microorganisms (pico-nanoplankton and bacteria, data not shown). Using our preferred  
 165 small addition of 0.2 nM, consumption of  $^{55}\text{Fe}$  during our incubations was negligible (1-4% of  
 166 total  $^{55}\text{Fe}$  added), and the consumption of the corresponding total dissolved Fe even smaller.

167 The Fe uptake rate ( $\text{mol Fe L}^{-1} \text{d}^{-1}$ ) noted  $\rho\text{Fe}$  (all symbols are listed in Table 2) was  
 168 calculated following the equations:

$$169 \quad \rho\text{Fe} = \frac{A \times ^{55}\text{Fe on filter}}{t \times V} \quad (1)$$

170 with

$$171 \quad A = \frac{\text{mol}^{55}\text{Fe added} + \text{mol DFe in situ}}{\text{mol}^{55}\text{Fe added}} \quad (2)$$

$$172 \quad ^{55}\text{Fe on filter} = \frac{(\text{cpm on filter sample} - \text{cpm on filter control})}{^{55}\text{Fe specific activity}} \times \frac{1}{\text{counting efficiency}} \quad (3)$$

173  $V$  = volume filtered

174  $t$  = incubation time

175 cpm = counts per minute

## 176 **2.5. Enumeration of heterotrophic bacteria**

177 Subsamples for cell enumeration were taken at the start and at the end of the  
 178 incubations. To enumerate heterotrophic bacteria, 2 mL samples were fixed with  
 179 glutaraldehyde (1% final concentration), incubated for 1h at 4°C, and stored at -80°C until

180 processed (Obernosterer et al., 2008). Heterotrophic bacterial cell abundance was counted  
181 with the FASCCanto II BD flow cytometer (Becton, Dickinson). Heterotrophic bacterial cells  
182 were stained with SYBRGreen I (Marie et al., 1997) and enumerated for 1 minute at a rate of  
183 30  $\mu\text{L min}^{-1}$ . The machine drift was tested using calibration beads (3  $\mu\text{m}$ ). Specific bacterial  
184 growth rates were calculated from the slope of log-linear regression between the start and the  
185 end of the incubation.

## 186 **2.6. Carbon content of different microbial size-fractions**

187 The cellular carbon content for heterotrophic bacteria was estimated to be 12.4 fgC per  
188 cell as reported by Fukuda et al. (1998). The carbon contents for pico-nanoplankton and  
189 microplankton were estimated from particulate organic carbon (POC) measured in surface  
190 seawater ( $< 1000 \mu\text{m}$ ) on 300, 210, 50, 20, 5, and 1  $\mu\text{m}$  pore-size filters (see Trull et al. 2014).  
191 We assumed the total carbon biomass (representative of the bulk community) to be the sum of  
192 all these fractions plus the estimated carbon biomass for heterotrophic bacteria. For pico-  
193 nanoplankton we assumed the sum of the POC concentrations on the 1 and 5 $\mu\text{m}$  filters,  
194 corresponding to the 1-20  $\mu\text{m}$  size-fraction, to be representative of this community. To obtain  
195 the carbon biomass for microplankton we subtracted the POC concentration of the 0.2-20  $\mu\text{m}$   
196 size-fraction of the total carbon biomass.

## 197 **3. RESULTS**

### 198 **3.1. Bulk iron uptake rates and contribution of different size-fractions**

199 The Fe uptake rate ( $\rho\text{Fe}$ ) for the bulk community, determined from incubations of  
200 unfiltered seawater (Fig. 2a), was measured at stations A3-2, E-4E and E-5, and the  
201 volumetric and integrated values are presented on Tables 3 and 4, respectively. The  
202 integration of  $\rho\text{Fe}$  over the euphotic layer reveals highest values at station E-5 (1.74  $\mu\text{mol Fe}$

203  $\text{m}^{-2} \text{d}^{-1}$ ), decreasing to  $1.12 \mu\text{mol Fe m}^{-2} \text{d}^{-1}$  at station A3-2 and to  $0.86 \mu\text{mol Fe m}^{-2} \text{d}^{-1}$  at  
204 station E-4E (Table 4). At these three stations the contribution of heterotrophic bacteria to  
205 total  $\rho\text{Fe}$  was less than 2% corresponding to a mean daily integrated uptake of  $0.018 \pm 0.005$   
206  $\mu\text{mol m}^{-2} \text{d}^{-1}$  (Table 4). The contribution of the two other size-fractions was station-dependent  
207 (Fig. 3). At station E-4E microplankton and pico-nanoplankton had almost equal contributions  
208 to total integrated  $\rho\text{Fe}$  (53% and 46%, respectively). At station A3-2 microplankton and pico-  
209 nanoplankton accounted for 40% and 59% of total integrated  $\rho\text{Fe}$ , respectively. The  
210 contribution of microplankton was the highest at station E-5 (69% of total integrated  $\rho\text{Fe}$ ),  
211 whereas the contribution of pico-nanoplankton was the lowest (29% of total integrated  $\rho\text{Fe}$ ) at  
212 this site.

213 To account for differences in the biomass among stations, we normalized  $\rho\text{Fe}$  to the  
214 concentration of POC of the microplankton and pico-nanoplankton size-classes and to the  
215 estimated cellular carbon content for bacteria, and both ratios are referred to  $\rho\text{Fe}:\text{POC}$  (Table  
216 3). For the bulk community, a trend similar to  $\rho\text{Fe}$  was observed, with the highest  $\rho\text{Fe}:\text{POC}$  at  
217 station E-5 ( $5.3 \pm 1.1 \mu\text{mol Fe d}^{-1} \text{mol C}^{-1}$ ;  $n=3$ , mean  $\pm 1$  SD of the three PAR levels),  
218 decreasing to  $3.0 \pm 1.0$  and  $2.5 \pm 0.4 \mu\text{mol Fe d}^{-1} \text{mol C}^{-1}$  ( $n=3$ , mean  $\pm 1$  SD) at stations A3-2  
219 and E-4E, respectively. Because this variability in  $\rho\text{Fe}:\text{POC}$  could in part reflect differences in  
220  $\rho\text{Fe}$  and carbon biomass contribution of organisms, we also considered  $\rho\text{Fe}:\text{POC}$  for the  
221 different size classes. At station E-5 microplankton revealed the highest  $\rho\text{Fe}:\text{POC}$  ratios  
222 ( $5.25$ - $11.56 \mu\text{mol Fe d}^{-1} \text{mol C}^{-1}$ ), while at station A3-2 pico-nanoplankton was highest ( $4.39$ -  
223  $7.03 \mu\text{mol Fe d}^{-1} \text{mol C}^{-1}$ ). At station E-5, at 75% of PAR, microplankton revealed the highest  
224  $\rho\text{Fe}:\text{POC}$  of all observed values. This is driven by the Fe uptake rate because carbon biomass  
225 was almost equally partitioned between microplankton (47 % of total carbon biomass) and  
226 pico-nanoplankton (44 % of total carbon biomass). Heterotrophic bacterial  $\rho\text{Fe}:\text{POC}$  was  
227 quite homogeneous in incubations at different PAR levels at stations E-4E ( $0.49 \pm 0.04 \mu\text{mol}$

228 Fe d<sup>-1</sup> mol C<sup>-1</sup>) and E-5 (0.73 ± 0.07 μmol Fe d<sup>-1</sup> mol C<sup>-1</sup>), but it presented high variability at  
229 station A3-2, ranging from 0.21 to 1.69 μmol Fe L<sup>-1</sup> d<sup>-1</sup> mol C<sup>-1</sup> (Table 3). As expected, due to  
230 the low contribution of heterotrophic bacteria to total ρFe, their carbon-normalized ρFe was  
231 the lowest among the three size-fractions.

### 232 **3.2. Heterotrophic bacterial iron uptake in the absence of phytoplankton**

233 To investigate whether heterotrophic bacteria compete with other members of the  
234 microbial community for the access to Fe, the bacterial Fe uptake rates and the bacterial  
235 growth rates were also determined during incubations where microplankton and both  
236 microplankton and pico-nanoplankton were excluded (experiments (b) and (c) respectively in  
237 Fig. 2). The bacterial Fe uptake rates were denoted  $(\rho Fe)_{bact}^{whole}$  if incubated with the whole  
238 community,  $(\rho Fe)_{bact}^{<25\mu m}$  if incubated with pico-nanoplankton only, while  $(\rho Fe)_{bact}^{alone}$  refers to  
239 bacterial Fe uptake rates measured when bacteria were incubated alone, with neither micro  
240 nor pico-nanoplankton. Incubations without microplankton were performed at 6 different light  
241 levels. At any given station, the variability of  $(\rho Fe)_{bact}^{<25\mu m}$  determined at different light levels  
242 did not exceed a factor of 4 (Table 5). The unique noticeable exception was station E-3 where  
243  $(\rho Fe)_{bact}^{<25\mu m}$  was about two orders of magnitude higher at 75% light level. To compare  
244  $(\rho Fe)_{bact}^{<25\mu m}$  among stations we integrated over the euphotic layer and the mixed layer depths.  
245 The outlier value at E-3 (at 75% PAR level) was not considered for the integration. The  
246 lowest depth-integrated values were observed at stations R-2 and E-5 (4.7 nmol Fe m<sup>-2</sup> d<sup>-1</sup> at  
247 both stations; mean of euphotic and mixed layer integrated fluxes) and the highest values  
248 were observed at station E-3 (18.4 nmol Fe m<sup>-2</sup> d<sup>-1</sup>). Integrated Fe uptake did not show any  
249 clear temporal evolution for the stations at the quasi Lagrangien time series E-2, E-3, E-4E  
250 and E-5 (Table 5).

251 The bacterial Fe uptake rate normalized to cellular carbon content was also determined  
252 in the incubations where microplankton was excluded (noted  $(\rho Fe: POC)_{bact}^{<25\mu m}$  in Table 5).  
253 The high value of  $(\rho Fe)_{bact}^{<25\mu m}$  measured at E-3 (at 75% PAR level) resulted in a high value  
254 of  $(\rho Fe: POC)_{bact}^{<25\mu m}$  (21.4  $\mu\text{mol Fe d}^{-1} \text{mol C}^{-1}$ ) that is considered as an outlier. All other  
255 values ranged from 0.06 to 2.94  $\mu\text{mol Fe d}^{-1} \text{mol C}^{-1}$ , and they were 2 to 8-fold lower than  
256 those in the corresponding incubations with the bulk community  $(\rho Fe: POC)_{bact}^{whole}$  (Stations  
257 A3-2, E-4E, and E-5). The normalization does not modify our general observation that there  
258 was no significant difference in the rates between the different light levels and between the  
259 different stations (two-tailed, unpaired Student's t-test,  $p=0.27$ ). In consideration of this, the  
260 values at one given station are now treated as biological replicates.

261 At the three stations A3-2, E-4E and E-5 we compared the bacterial Fe uptake when  
262 bacteria were incubated with the whole community  $((\rho Fe: POC)_{bact}^{whole})$  with that when  
263 incubated with pico-nanoplankton only  $((\rho Fe: POC)_{bact}^{<25\mu m})$  and that with bacteria alone  
264  $((\rho Fe: POC)_{bact}^{alone})$ , Fig. 4). For all stations, we found that bacterial Fe uptake was the highest  
265 in the absence of any other larger cells and the lowest when incubated with pico-nanoplankton  
266 only, with  $(\rho Fe: POC)_{bact}^{alone} > (\rho Fe: POC)_{bact}^{whole} > (\rho Fe: POC)_{bact}^{<25\mu m}$ . When bacteria were  
267 incubated with the entire microbial community,  $(\rho Fe: POC)_{bact}^{whole}$  was 2 to 8 times higher than  
268 in the incubations with pico-nanoplankton only  $((\rho Fe: POC)_{bact}^{<25\mu m})$ , but still lower than when  
269 bacteria were incubated alone. Similarly to  $(\rho Fe: POC)_{bact}^{alone}$ , bacterial growth rates were by 2  
270 to 5 times higher when bacteria were incubated alone compared to incubations with pico-  
271 nanoplankton only (Fig. 4b).

### 272 3.3. Growth rates and iron quota of heterotrophic bacteria

273 In all the incubation experiments the abundance of heterotrophic bacteria was  
274 determined at the beginning and at the end of the incubation period. Assuming an exponential

275 growth during the incubation provided an estimate of the growth rates. The lowest growth rate  
276 ( $0.02 \text{ d}^{-1}$ ) was determined at the station R-2. For the other stations, the growth rate ranged  
277 from  $0.12 \text{ d}^{-1}$  (E-5) to  $0.36 \text{ d}^{-1}$  (E-3). We also measured  $(\rho Fe: POC)_{bact}^{alone}$  after 24, 72, 96 h and  
278 after 7 days of incubation. The  $(\rho Fe: POC)_{bact}^{alone}$  was similar after 24h and 96h of incubation  
279 and decreased after one week of incubation (data not shown). This suggests that 24h of  
280 incubation provides a measurement of steady state Fe uptake rate. Thus, we derived the Fe  
281 quota for heterotrophic bacteria ( $Q_{Fe}$ ) based on the equation  $\rho = \mu Q_{Fe}$  (Fig. 5). The Fe quota of  
282 heterotrophic bacteria was  $4 \times 10^{-20} \text{ mol Fe cell}^{-1}$  for stations R-2, E-5, and E-4W, and  $8 \times 10^{-20}$   
283  $\text{mol Fe cell}^{-1}$  for station E-2, F-L, A3-2 and E-3.

## 284 **4. DISCUSSION**

### 285 **4.1. The microbial Fe demand**

286 In the vicinity of the Kerguelen Islands, natural Fe fertilization produces many blooms  
287 with different dynamics resulting from a combination of hydrodynamic and ecological  
288 drivers. These sites provide excellent opportunities to investigate the demand of different  
289 members of the microbial community for Fe, and how these members interact. During the  
290 project KEOPS2 we visited a variety of early spring blooms located above the Kerguelen  
291 plateau and in offshore waters north and south of the Polar Front. We start our discussion by  
292 putting our results in the context of previous studies related to Fe uptake by the microbial  
293 community in the Southern Ocean.

294 In the early spring bloom located above the Kerguelen Plateau (station A3-2), the total Fe  
295 demand, defined here as the steady state Fe uptake rate by the bulk community, was  $33.2$   
296  $\text{pmol Fe L}^{-1} \text{ d}^{-1}$  in surface waters. This Fe demand is more than 6 times higher than that  
297 determined during KEOPS1 at the same site during the declining phase of the bloom ( $5.3 \pm 1.2$   
298  $\text{pmol L}^{-1} \text{ d}^{-1}$  for a mean value of A3-4 and A3-5, 50% of PAR, Sarthou et al., 2008). The Fe

299 demand during KEOPS2 is also higher than that measured during the artificial Fe fertilization  
300 experiment SOIREE in the Antarctic zone. At about 13 days following the Fe addition, a  
301 time-point which corresponded to the growing phase of the bloom, Bowie et al.,(2001)  
302 determined an Fe demand of  $11.9 \text{ pmol L}^{-1} \text{ d}^{-1}$  (mean mixed layer). The differences in the Fe  
303 demand between these three studies likely do not result from differences in biomass, because  
304 POC concentrations in the surface mixed layer were similar between studies (10-12  $\mu\text{M}$ ;  
305 Bowie et al., 2001; Sarthou et al., 2008; Trull et al., 2014).

306 For the KEOPS expeditions, different stages of the bloom provide a temporal framework  
307 to interpret these observations. However, this is not the case for the differences observed  
308 between KEOPS2 and SOIREE, which were both sampled during the early phase of a bloom,  
309 even if the blooms occurred at different seasons. Besides the seasonal differences, the location  
310 of the study could explain the variability in the Fe demand. Finally, the results of FeCycle  
311 provide a comparison with the Sub Antarctic zone. The Fe demand determined for the steady-  
312 state microbial Fe budget was 26-101  $\text{pmol L}^{-1} \text{ d}^{-1}$ , (Strzepek et al., 2005), thus at the upper  
313 bound or higher than during KEOPS2, although carbon biomasses were similar (10.2  $\mu\text{M}$ ,  
314 average for the mixed layer). From all these comparisons it appears that besides the variability  
315 driven by temporal or spatial factors, a plankton-based mechanistic explanation is certainly  
316 required for a better understanding of the observed differences.

317 Culture studies (Marchetti et al., 2009; Strzepek and Harrison, 2004; Sunda and  
318 Huntsman, 1995, 1997) or molecular approaches (Allen et al., 2008) have shown that there  
319 are multiple strategies for phytoplankton to deal with Fe limitation. The consequences are that  
320 bulk cell properties like the Fe uptake rate, the intracellular Fe concentration or the elemental  
321 Fe:C ratio are species dependent. However, the use of this basic knowledge to interpret field  
322 results is not straightforward. This is primarily due to the complexity of the natural  
323 phytoplankton community, but it is also obscured by possible regional differences as shown

324 by Strzepek et al. (2012). Southern Ocean phytoplankton species responded to Fe-light  
325 acclimation differently than temperate species (Sunda and Huntsman, 1997; Strzepek et al.,  
326 2012). In the case of heterotrophic bacteria, culture studies (Armstrong et al., 2004; Fourquez  
327 et al., 2014; Granger and Price, 1999) and metagenomic analysis (Hopkinson and Barbeau,  
328 2012; Toulza et al., 2012) have also provided foundations for our understanding of the  
329 responses of bacteria to Fe limitation but extrapolation to field observations face the same  
330 constraints as mentioned for phytoplankton.

331 A step forward to obtain some insight into the role of the community composition is to  
332 compare parameters in different size-fractions. In Fe-fertilized systems in the Southern Ocean,  
333 the largest size-fraction ( $> 25 \mu\text{m}$ ), named microplankton, is almost entirely composed of  
334 diatoms. In the early spring bloom above the Kerguelen plateau, this fraction contributed 40%  
335 of the total Fe uptake. This is substantially lower than during the declining phase of the bloom  
336 where 62 % of total Fe uptake was accounted for by microplankton (Sarhou et al. 2008). This  
337 decrease in the contribution of microplankton is consistent with the idea that the early phase  
338 of the bloom is dominated by a succession of rapidly growing diatoms of different sizes, and  
339 that larger slow growing, and silicon limited diatoms accumulate at the end of the season  
340 (Quéguiner, 2013). At the onset of the bloom above the plateau, pico-nanoplankton were the  
341 main contributor to Fe uptake (69%) and this size-fraction also revealed the highest carbon-  
342 normalized Fe uptake rates. This fraction contains mainly small diatoms because non-diatom  
343 phytoplankton, as determined by flow cytometry, had a minor contribution to POC in this  
344 size-fraction at station A3-2 ( $7.4 \pm 0.4 \%$ ,  $n=6$ ). This suggests that the diatoms belonging to  
345 this size class are more competitive than larger cells for the conditions prevailing at this  
346 period of the season. The same observation holds for the FeCycle experiment in the Sub-  
347 Antarctic where the Fe uptake was dominated by photosynthetic pico-nanoplankton during  
348 the early bloom ( Strzepek et al., 2005, Boyd and Ellwood, 2010).

349 In addition to  $\rho\text{Fe}:\text{POC}$ , we have also calculated the Fe:C uptake ratios based on *in situ*  
350 primary production measurements (Cavagna et al., 2014). In the Southern Ocean, Fe:C uptake  
351 ratios (noted here  $\rho\text{Fe}:\rho\text{C}$ ) reported in the literature range from  $\sim 5$  to  $50 \mu\text{mol Fe mol C}^{-1}$   
352 (Sarhou et al., 2005 and references herein) and can reach up to  $100 \mu\text{mol Fe mol C}^{-1}$ , as it  
353 was reported in some artificial Fe fertilizations (Boyd et al., 2000). During KEOPS2, the  
354  $\rho\text{Fe}:\rho\text{C}$  ranged from 3.7 (station A3-2) to  $22.9 \mu\text{mol Fe mol C}^{-1}$  (station E-5, Fig. 6). The  
355 values determined for the plateau station A3-2 ( $3.7\text{-}11 \mu\text{mol Fe mol C}^{-1}$ ) are similar to those  
356 reported for the declining phase of the bloom during KEOPS1 ( $5.0 \pm 2.6 \mu\text{mol Fe mol C}^{-1}$ ,  
357 average for stations A3-1, A3-4, and A3-5, Sarhou et al., 2008). These  $\rho\text{Fe}:\rho\text{C}$  ratios are also  
358 consistent with values measured during the two FeCycle studies where  $\rho\text{Fe}:\rho\text{C}$  were  
359 comprised between 5.5 and  $19 \mu\text{mol Fe mol C}^{-1}$ , and did not vary much with depth and over  
360 time (King et al., 2012; Strzepek et al., 2005). By contrast, at the stations located downstream  
361 of the plateau (E-4E and E-5) the  $\rho\text{Fe}:\rho\text{C}$  values were overall higher than above the plateau  
362 (range 10 to  $22 \mu\text{mol Fe mol C}^{-1}$ ).

#### 363 **4.2. Phytoplankton- bacteria competition for iron acquisition**

364 During KEOPS2, heterotrophic bacteria contributed less than 2% to the total Fe uptake  
365 ( $\rho\text{Fe}$ ). This is similar to the low contribution of heterotrophic bacteria of 1 to 5% to the total  
366  $\rho\text{Fe}$  during FeCycle (Strzepek et al., 2005), but contrasts with observations from the subarctic  
367 Pacific where heterotrophic bacteria dominated the Fe uptake (20-45%, Tortell et al., 1996).  
368 Heterotrophic bacterial Fe uptake was negatively affected by the presence of pico- to  
369 microplankton, suggesting competition between these members of the microbial community.  
370 Competition for the limiting nutrient is not unexpected, however, this issue has rarely been  
371 addressed in previous studies (Boyd et al., 2012). Bacterial and pico-nanoplanktonic cells  
372 could compete for nutrients as both have comparable metabolic rates (Massana and Logares,

373 2012), and high capacities for resource acquisition. Our observation of the overall low  
374 contribution of heterotrophic bacteria to bulk Fe uptake suggests that not only the access to  
375 Fe, but also organic carbon could have limited the bacterial response to natural Fe  
376 fertilization. This idea is supported by the relation between the extent of stimulation of  
377 bacterial Fe uptake in fertilized waters and the increase in primary production (Fig. 7).

378 The bacterial Fe uptake rates were highest when measured in the absence of any larger  
379 cells and lowest in incubations where microplankton was excluded and bacteria were  
380 incubated with pico-nanoplankton only (Fig. 4a). This was the case for all stations where the  
381 experiment was conducted with  $(\rho Fe: POC)_{bact}^{alone}$  5 to 26 times higher than  $(\rho Fe: POC)_{bact}^{<25\mu m}$ ,  
382 except for the reference station R-2. Considering that a higher degree of Fe limitation should  
383 result in an increased cellular Fe uptake rate, raises the question of whether different degrees  
384 of Fe limitation of bacteria and pico-nanoplankton could explain the observed pattern. To  
385 evaluate the degree of Fe limitation, we compared bacterial and pico-nanoplankton Fe uptake  
386 rates (Table 6). Two clear features emerge. First, Fe uptake rates for bacteria  
387  $((\rho Fe: POC)_{bact}^{alone})$  and pico-nanoplankton  $((\rho Fe: POC)_{pico-nano})$  are very similar for a given  
388 station, suggesting that they experienced comparable degree of Fe limitation before the  
389 beginning of the incubation experiment. Second, the bacterial Fe uptake rates when incubated  
390 alone  $((\rho Fe: POC)_{bact}^{alone})$  are higher in fertilized waters than at the HNLC site, suggesting that  
391 bacteria are not Fe replete at the fertilized stations. The strong correlation between C-  
392 normalized bacterial Fe uptake rates when incubated alone and primary production (n=5,  
393  $r^2=0.97$  and  $p=0.002$ , Fig. 7), suggests that carbon availability is the main driver of the Fe  
394 uptake potential of heterotrophic bacteria. Interestingly, no such correlation was obtained  
395 when bacteria were incubated with pico-nanoplankton only (n=5,  $r^2= 0.31$  and  $p=0.32$ ). These  
396 observations strongly suggest that for the stations located in Fe-fertilized regions,

397 phytoplankton, and in particular pico-nanoplankton, competed with bacteria for Fe  
398 acquisition.

399 We propose two non-exclusive explanations for the observed positive correlation between  
400 these two parameters. First, the increase in primary production could be driven by an increase  
401 in Fe availability that may also benefit heterotrophic bacteria when competition with larger  
402 cells is alleviated. Second, the increase in primary production could result in an enhanced  
403 amount of phytoplankton-derived DOC, which in turn provides energy to synthesize more  
404 iron transport molecules to cope with a certain degree of Fe limitation and also stimulates the  
405 bacterial Fe demand. In the absence of microplankton, the supply of phytoplankton-DOM is  
406 likely to be lower, which could explain the strong decrease in bacterial Fe uptake rates in  
407 these incubations  $(\rho Fe: POC)_{bact}^{<25\mu m}$ . Both mechanisms are likely to occur, as independent  
408 experiments during KEOPS2 revealed that bacterial production was stimulated by both, single  
409 additions of Fe and organic carbon (Obernosterer et al., 2014).

410 DOC is undoubtedly one of the most important substrates provided by autotrophic  
411 phytoplankton cells to heterotrophic bacteria. The amount of DOC produced by  
412 phytoplankton during the bloom is likely to play a role in Fe demand by bacteria. Kirchman et  
413 al., (2000) suggested that low Fe availability leads to increase the C demand and more  
414 recently, Fourquez et al., (2014) have provided some evidence that marine heterotrophic  
415 bacteria reallocate their inner resources to sustain this increase of the C demand when Fe  
416 limited. Here, we also show that high C availability leads to an increase in Fe demand. Finally  
417 we note that the minimum values of  $(\rho Fe: POC)_{bact}^{<25\mu m}$  in comparison to whole community  
418  $(\rho Fe: POC)_{bact}^{whole}$  and bacteria-only  $(\rho Fe: POC)_{bact}^{alone}$  incubations could arise via other  
419 microorganism allelopathic interaction mechanisms than competition for Fe. As such, further

420 research is needed to examine interactions between pico-nanoplankton and bacteria across a  
421 wider range of conditions, i.e. including non-limiting Fe and carbon substrate levels.

422 Our observation that small diatoms were particularly competitive in removing Fe during  
423 the early stage of the spring phytoplankton bloom induced by natural Fe-fertilization in the  
424 Southern Ocean suggests an intimate connection between heterotrophic bacteria and pico-  
425 nanoplankton. If this is the case, a progressive shift in the community composition from small  
426 to larger diatoms in the course of a bloom (Quéguiner, 2013) would affect the bacterial Fe  
427 uptake rates over time. This could partly explain why heterotrophic bacteria accounted for 17-  
428 27% of the overall Fe-uptake at the late stage of the spring bloom (Sarhou et al., 2008) in  
429 contrast to 1-2% at the onset of the bloom. Together, these results demonstrate that the  
430 bacterial Fe and carbon metabolism are closely coupled, and that the structure of the microbial  
431 community has a marked effect on the extent of bacterially-mediated Fe cycling.

432 **Figure captions**

433 **Figure 1**

434 Map of KEOPS2 study area showing the stations sampled for Fe uptake experiments. Dashed  
435 line represents the position of the Polar Front. The base map shows the bathymetry in meters.

436 **Figure 2**

437 Schematic representation of experiments to determine Fe uptake by heterotrophic bacteria  
438 (0.2-0.8  $\mu\text{m}$ ), pico-nanoplankton (0.8-25  $\mu\text{m}$ ) and microplankton ( $>25 \mu\text{m}$ ) during the  
439 KEOPS2 cruise (sw for seawater).

440 **Figure 3**

441 Relative contribution of different size-fractions to total Fe uptake ( $\rho\text{Fe}$ ). The percent  
442 contribution was calculated from Fe uptake fluxes integrated over the euphotic layer at  
443 plateau (A3-2) and downstream plume (E-4E and E-5) stations.

444 **Figure 4**

445 Bacterial Fe uptake normalized per carbon biomass (a) and bacterial growth rates (b) in  
446 incubations conducted with whole community ( $(\rho\text{Fe}: \text{POC})_{bact}^{whole}$ , unfiltered seawater), with  
447 pico-nanoplankton only ( $(\rho\text{Fe}: \text{POC})_{bact}^{<25\mu\text{m}}$ , 25  $\mu\text{m}$  prefiltered seawater), and when bacteria  
448 were incubated alone ( $(\rho\text{Fe}: \text{POC})_{bact}^{alone}$ , 0.8  $\mu\text{m}$  prefiltered seawater). As no significant effect  
449 of light on Fe uptake was observed for any station we consider the values measured at the  
450 different levels of PAR as replicates. The bars for unfiltered seawater represent the average  $\pm$   
451 1 SD of the three light levels (75%, 25% and 1% of surface PAR). The bars for  $<25 \mu\text{m}$   
452 seawater represent the average  $\pm$  1 SD of all the light levels (n=6 for stations E-4E, E-5, and  
453 E-4W; n=5 for stations A3-2 and R-2).

454 **Figure 5**

455 Relationship between the intracellular bacterial Fe quota and growth rate. Black squares:  
456 Station E-4W, E-5 and R-2 stations; regression line  $r^2=0.99$ ,  $y=4.8 \times 10^{-14} + 8.9 \times 10^{-15}$ . Grey  
457 circles: Station E-2, E-3, A3-2, and F-L stations; regression line  $r^2=0.99$ ,  $y=10 \times 10^{-14} + 1.4 \times 10^{-15}$ .  
458 Calculations are based on bacterial Fe uptake and growth rates measured when incubated  
459 with pico-nanoplankton only.

460 **Figure 6**

461 Comparison between total Fe:C uptake ratios noted  $\rho\text{Fe}:\rho\text{C}$  (black bars) and Fe uptake by the  
462 bulk community normalized to carbon biomass noted  $\rho\text{Fe}:\text{POC}$  (grey bars) at 3 different  
463 surface PAR levels at stations A3-2 (plateau), E-4E and E-5 (plume).

464 **Figure 7**

465 Relationship between the C-normalized bacterial Fe uptake ( $(\rho\text{Fe}:\text{POC})_{bact}^{alone}$ ) and euphotic  
466 zone integrated primary production. The plotted line was obtained by least-square regression  
467 ( $r^2=0.97$  with  $p=0.002$ ). Empty symbol represents the reference station R-2 and filled symbols  
468 are for Fe-fertilized stations.

469 **Acknowledgments**

470 We would like to thanks the captain Bernard Lassiette, the chief scientist Bernard Quéguiner,  
471 and the crew of the R/V Marion-Dufresne II for assistance on board. We want to acknowledge  
472 gratefully Emmanuel Laurenceau-Cornec for making the satellite chlorophyll animation  
473 available and Laurent Besnard for his assistance in creating Figure 1. We thank two  
474 anonymous reviewers who helped to improve a previous version of the manuscript. This work  
475 was supported by the French Research program of INSU-CNRS LEFE-CYBER (Les  
476 enveloppes fluides et l'environnement –Cycles biogéochimiques, environnement et  
477 ressources), the French ANR (Agence Nationale de la Recherche, SIMI-6 program, ANR-10-  
478 BLAN-0614), the French CNES (Centre National d'Etudes Spatiales) and the French Polar  
479 Institute IPEV (Institut Polaire Paul-Emile Victor).

480 **References**

- 481 Allen, A. E., Laroche, J., Maheswari, U., Lommer, M., Schauer, N., Lopez, P. J., Finazzi, G.,  
482 Fernie, A. R. and Bowler, C.: Whole-cell response of the pennate diatom *Phaeodactylum*  
483 *tricornutum* to iron starvation., *Proc. Natl. Acad. Sci. U. S. A.*, 105(30), 10438–10443,  
484 doi:10.1073/pnas.0711370105, 2008.
- 485 Amin, S. A., Green, D. H., Hart, M. C., Küpper, F. C., Sunda, W. G., Carrano, C. J. and Ku,  
486 F. C.: Photolysis of iron – siderophore chelates promotes bacterial – algal mutualism, *Proc.*  
487 *Natl. Acad. Sci. U. S. A.*, 106(40), 17071–17076, doi:10.1073/pnas.0905512106, 2009.
- 488 Armstrong, E., Granger, J., Mann, E. L. and Price, N. M.: Outer-membrane siderophore  
489 receptors of heterotrophic oceanic bacteria, *Limnol. Oceanogr.*, 49(2), 579–587,  
490 doi:10.4319/lo.2004.49.2.0579, 2004.
- 491 Arrigo, K. R.: Molecular diversity and ecology of microbial plankton., *Nature*, 437(7057),  
492 343–348, doi:10.1038/nature04158, 2005.
- 493 Blain, S., Capparas, J., Guéneuguès, A., Obernosterer, I. and Oriol, L.: Distributions and  
494 stoichiometry of dissolved nitrogen and phosphorus in the iron fertilized region near  
495 Kerguelen (Southern Ocean), *Biogeosciences*, 11(6), 9949–9977, doi:10.5194/bgd-11-9949-  
496 2014, 2014.
- 497 Blain, S., Quéguiner, B., Armand, L., Belviso, S., Bombled, B., Bopp, L., Bowie, A., Brunet,  
498 C., Brussaard, C., Carlotti, F., Christaki, U., Corbière, A., Durand, I., Ebersbach, F., Fuda, J.-  
499 L., Garcia, N., Gerringa, L., Griffiths, B., Guigue, C., Guillerm, C., Jacquet, S., Jeandel, C.,  
500 Laan, P., Lefèvre, D., Lo Monaco, C., Malits, A., Mosseri, J., Obernosterer, I., Park, Y.-H.,  
501 Picheral, M., Pondaven, P., Remenyi, T., Sandroni, V., Sarthou, G., Savoye, N., Scouarnec,  
502 L., Souhaut, M., Thuiller, D., Timmermans, K., Trull, T., Uitz, J., van Beek, P., Veldhuis, M.,  
503 Vincent, D., Viollier, E., Vong, L. and Wagener, T.: Effect of natural iron fertilization on  
504 carbon sequestration in the Southern Ocean., *Nature*, 446(7139), 1070–1074,  
505 doi:10.1038/nature05700, 2007.
- 506 Bowie, A. R., Maldonado, M. T., Frew, R. D., Croot, P. L., Achterberg, E. P., Mantoura, R. F.  
507 C., Worsfold, P. J., Law, C. S. and Boyd, P. W.: The fate of added iron during a mesoscale  
508 fertilisation experiment in the Southern Ocean, *Deep Sea Res. Part II Top. Stud. Oceanogr.*,  
509 48(11-12), 2703–2743, doi:10.1016/S0967-0645(01)00015-7, 2001.
- 510 Bowie, A. R., van der Merwe, P., Quéroué, F., Trull, T., Fourquez, M., Planchon, F., Sarthou,  
511 G., Chever, F., Townsend, A. T., Obernosterer, I., Sallée, J.-B. and Blain, S.: Iron budgets for  
512 three distinct biogeochemical sites around the Kerguelen archipelago (Southern Ocean)  
513 during the natural fertilisation experiment KEOPS-2, *Biogeosciences Discuss.*, 11(12),  
514 17861–17923, doi:10.5194/bgd-11-17861-2014, 2014.
- 515 Boyd, P. W. and Ellwood, M. J.: The biogeochemical cycle of iron in the ocean, *Nat. Geosci.*,  
516 3(10), 675–682, doi:10.1038/ngeo964, 2010.
- 517 Boyd, P. W., Strzpek, R., Chiswell, S., Chang, H., DeBruyn, J. M., Ellwood, M., Keenan, S.,  
518 King, A. L., Maas, E. W., Nodder, S., Sander, S. G., Sutton, P., Twining, B. S., Wilhelm, S.

- 519 W. and Hutchins, D. a.: Microbial control of diatom bloom dynamics in the open ocean,  
520 *Geophys. Res. Lett.*, 39(18), 1–6, doi:10.1029/2012GL053448, 2012.
- 521 Boyd, P. W., Watson, A. J., Law, C. S., Abraham, E. R., Trull, T., Murdoch, R., Bakker, D.  
522 C., Bowie, A. R., Buesseler, K. O., Chang, H., Charette, M., Croot, P., Downing, K., Frew,  
523 R., Gall, M., Hadfield, M., Hall, J., Harvey, M., Jameson, G., LaRoche, J., Liddicoat, M.,  
524 Ling, R., Maldonado, M. T., McKay, R. M., Nodder, S., Pickmere, S., Pridmore, R., Rintoul,  
525 S., Safi, K., Sutton, P., Strzepek, R. F., Tanneberger, K., Turner, S., Waite, A. and Zeldis, J.:  
526 A mesoscale phytoplankton bloom in the polar Southern Ocean stimulated by iron  
527 fertilization., *Nature*, 315(5812), 612–617, doi:10.1038/35037500, 2000.
- 528 Cavagna, a. J., Fripiat, F., Elskens, M., Dehairs, F., Mangion, P., Chirurgien, L., Closset, I.,  
529 Lasbleiz, M., Flores–Leiva, L., Cardinal, D., Leblanc, K., Fernandez, C., Lefèvre, D., Oriol,  
530 L., Blain, S. and Quéguiner, B.: Biological productivity regime and associated N cycling in  
531 the vicinity of Kerguelen Island area, Southern Ocean, *Biogeosciences Discuss.*, 11(12),  
532 18073–18104, doi:10.5194/bgd-11-18073-2014, 2014.
- 533 Closset, I., Lasbleiz, M., Leblanc, K., Quéguiner, B., Cavagna, a.-J., Elskens, M., Navez, J.  
534 and Cardinal, D.: Seasonal evolution of net and regenerated silica production around a natural  
535 Fe-fertilized area in the Southern Ocean estimated from Si isotopic approaches,  
536 *Biogeosciences Discuss.*, 11(5), 6329–6381, doi:10.5194/bgd-11-6329-2014, 2014.
- 537 d’Ovidio, F., Della Penna, A., Trull, T. W., Nencioli, F., Pujol, I., Rio, M. H., Park, Y.-H.,  
538 Cotté, C., Zhou, M. and Blain, S.: The biogeochemical structuring role of horizontal stirring:  
539 Lagrangian perspectives on iron delivery downstream of the Kerguelen plateau,  
540 *Biogeosciences Discuss.*, 12, 779–814, doi:10.5194/bgd-12-779-2015, 2015.
- 541 Fourquez, M., Devez, A., Schaumann, A., Guéneuguès, A., Jouenne, T., Obernosterer, I. and  
542 Blain, S.: Effects of iron limitation on growth and carbon metabolism in oceanic and coastal  
543 heterotrophic bacteria, *Limnol. Oceanogr.*, 59(2), 349–360, doi:10.4319/lo.2014.59.2.0349,  
544 2014.
- 545 Fourquez, M., Obernosterer, I. and Blain, S.: A method for the use of the radiotracer <sup>55</sup>Fe for  
546 microautoradiography and CARD-FISH of natural bacterial communities, *FEMS Microbiol.*  
547 *Lett.*, 337(2), 132–139, doi:10.1111/1574-6968.12022, 2012.
- 548 Fukuda, R., Ogawa, H., Nagata, T. and Koike, I.: Direct determination of carbon and nitrogen  
549 contents of natural bacterial assemblages in marine environments, *Appl. Environ. Microbiol.*,  
550 64(9), 3352–8, 1998.
- 551 Granger, J. and Price, N. M.: The importance of siderophores in iron nutrition of heterotrophic  
552 marine bacteria, *Limnol. Oceanogr.*, 44(3), 541–555, doi:10.4319/lo.1999.44.3.0541, 1999.
- 553 Hassler, C. S., Alasonati, E., Mancuso Nichols, C. A. and Slaveykova, V. I.:  
554 Exopolysaccharides produced by bacteria isolated from the pelagic Southern Ocean — Role  
555 in Fe binding, chemical reactivity, and bioavailability, *Mar. Chem.*, 123(1-4), 88–98,  
556 doi:10.1016/j.marchem.2010.10.003, 2011a.

557 Hassler, C. S., Schoemann, V., Nichols, C. M., Butler, E. C. V and Boyd, P. W.: Saccharides  
558 enhance iron bioavailability to Southern Ocean phytoplankton, *Proc. Natl. Acad. Sci. U. S.*  
559 *A.*, 108(3), 1076–1081, doi:10.1073/pnas.1010963108, 2011b.

560 Hopkinson, B. M. and Barbeau, K. A.: Iron transporters in marine prokaryotic genomes and  
561 metagenomes., *Environ. Microbiol.*, 14(1), 114–28, doi:10.1111/j.1462-2920.2011.02539.x,  
562 2012.

563 Hudson, R. J. M. and Morel, F. M. M.: Distinguishing between extra- and intracellular iron in  
564 marine phytoplankton, *Limnol. Oceanogr.*, 34(6), 1113–1120, doi:10.4319/lo.1989.34.6.1113,  
565 1989.

566 King, a. L., Sañudo-Wilhelmy, S. a., Boyd, P. W., Twining, B. S., Wilhelm, S. W., Breene,  
567 C., Ellwood, M. J. and Hutchins, D. a.: A comparison of biogenic iron quotas during a diatom  
568 spring bloom using multiple approaches, *Biogeosciences*, 9(2), 667–687, doi:10.5194/bg-9-  
569 667-2012, 2012.

570 Kirchman, D. L., Meon, B., Cottrell, M. T., Hutchins, D. a., Weeks, D. and Bruland, K. W.:  
571 Carbon versus iron limitation of bacterial growth in the California upwelling regime, *Limnol.*  
572 *Oceanogr.*, 45(8), 1681–1688, doi:10.4319/lo.2000.45.8.1681, 2000.

573 Lasbleiz, M., Leblanc, K., Blain, S., Ras, J., Cornet-Barthaux, V., Hélias Nunige, S. and  
574 Quéguiner, B.: Pigments, elemental composition (C, N, P, Si) and stoichiometry of particulate  
575 matter, in the naturally iron fertilized region of Kerguelen in the Southern Ocean,  
576 *Biogeosciences Discuss.*, 11(6), 8259–8324, doi:10.5194/bgd-11-8259-2014, 2014.

577 Litchman, E., Klausmeier, C. a. and Bossard, P.: Phytoplankton nutrient competition under  
578 dynamic light regimes, *Limnol. Oceanogr.*, 49(4\_part\_2), 1457–1462,  
579 doi:10.4319/lo.2004.49.4\_part\_2.1457, 2004.

580 Madsen, E. L.: Microorganisms and their roles in fundamental biogeochemical cycles., *Curr.*  
581 *Opin. Biotechnol.*, 22(3), 456–64, doi:10.1016/j.copbio.2011.01.008, 2011.

582 Maldonado, M. T., Boyd, P. W., LaRoche, J., Strzepek, R. F., Waite, A., Bowie, A. R., Croot,  
583 P. L., Frew, R. D. and Price, N. M.: Iron uptake and physiological response of phytoplankton  
584 during a mesoscale Southern Ocean iron enrichment, *Limnol. Oceanogr.*, 46(7), 1802–1808,  
585 doi:10.4319/lo.2001.46.7.1802, 2001.

586 Marchetti, A., Parker, M. S., Moccia, L. P., Lin, E. O., Arrieta, A. L., Ribalet, F., Murphy, M.  
587 E. P., Maldonado, M. T. and Armbrust, E. V.: Ferritin is used for iron storage in bloom-  
588 forming marine pennate diatoms., *Nature*, 457(7228), 467–470, doi:10.1038/nature07539,  
589 2009.

590 Marie, D., Partensky, F., Jacquet, S. and Vaultot, D.: Enumeration and cell cycle analysis of  
591 natural populations of marine picoplankton by flow cytometry using the nucleic acid stain  
592 SYBR Green I, *Appl. Environ. Microbiol.*, 63(1), 186–193, 1997.

593 Martin, J. H.: Glacial interglacial CO<sub>2</sub> change: the iron hypothesis, *Paleoceanography*, 5(1),  
594 1–13, doi:10.1029/PA005i001p00001, 1990.

- 595 Massana, R. and Logares, R.: Eukaryotic versus prokaryotic marine picoplankton ecology.,  
596 *Environ. Microbiol.*, 15(5), 1254–1261, doi:10.1111/1462-2920.12043, 2012.
- 597 Mills, M. M., Moore, C. M., Langlois, R., Milne, A., Achterberg, E. P., Nachtigall, K.,  
598 Lochte, K., Geider, R. J. and La Roche, J.: Nitrogen and phosphorus co-limitation of bacterial  
599 productivity and growth in the oligotrophic subtropical North Atlantic, *Limnol. Oceanogr.*,  
600 53(2), 824–834, doi:10.4319/lo.2008.53.2.0824, 2008.
- 601 Nielsdóttir, M. C., Bibby, T. S., Moore, C. M., Hinz, D. J., Sanders, R., Whitehouse, M.,  
602 Korb, R. and Achterberg, E. P.: Seasonal and spatial dynamics of iron availability in the  
603 Scotia Sea, *Mar. Chem.*, 130-131, 62–72, doi:10.1016/j.marchem.2011.12.004, 2012.
- 604 Obernosterer, I., Christaki, U., Lefevre, D., Catala, P., Vanwambeke, F. and Lebaron, P.:  
605 Rapid bacterial mineralization of organic carbon produced during a phytoplankton bloom  
606 induced by natural iron fertilization in the Southern Ocean, *Deep Sea Res. Part II*, 55(5-7),  
607 777–789, 2008.
- 608 Pollard, R. T., Salter, I., Sanders, R. J., Lucas, M. I., Moore, C. M., Mills, R. A., Statham, P.  
609 J., Allen, J. T., Baker, A. R., Bakker, D. C. E., Charette, M. a, Fielding, S., Fones, G. R.,  
610 French, M., Hickman, A. E., Holland, R. J., Hughes, J. A., Jickells, T. D., Lampitt, R. S.,  
611 Morris, P. J., Nédélec, F. H., Nielsdóttir, M., Planquette, H., Popova, E. E., Poulton, A. J.,  
612 Read, J. F., Seeyave, S., Smith, T., Stinchcombe, M., Taylor, S., Thomalla, S., Venables, H.  
613 J., Williamson, R. and Zubkov, M. V: Southern Ocean deep-water carbon export enhanced by  
614 natural iron fertilization., *Nature*, 457(7229), 577–580, doi:10.1038/nature07716, 2009.
- 615 Quéguiner, B.: Iron fertilization and the structure of planktonic communities in high nutrient  
616 regions of the Southern Ocean, *Deep Sea Res. Part II Top. Stud. Oceanogr.*, 90, 43–54,  
617 doi:10.1016/j.dsr2.2012.07.024, 2013.
- 618 Quéroué, F., Sarthou, G., Planquette, H. F., Bucciarelli, E., Chever, F., van der Merwe, P.,  
619 Lannuzel, D., Townsend, a. T., Cheize, M., Blain, S., d’Ovidio, F. and Bowie, a. R.: High  
620 variability of dissolved iron concentrations in the vicinity of Kerguelen Island (Southern  
621 Ocean), *Biogeosciences Discuss.*, 12(1), 231–270, doi:10.5194/bgd-12-231-2015, 2015.
- 622 Sarthou, G., Vincent, D., Christaki, U., Obernosterer, I., Timmermans, K. R. and Brussaard,  
623 C. P. D.: The fate of biogenic iron during a phytoplankton bloom induced by natural  
624 fertilisation: Impact of copepod grazing, *Deep Sea Res. Part II*, 55(5-7), 734–751,  
625 doi:10.1016/j.dsr2.2007.12.033, 2008.
- 626 Strzepek, R. F. and Harrison, P. J.: Photosynthetic architecture differs in coastal and oceanic  
627 diatoms, *Nature*, 403, 689–692, doi:10.1038/nature02954, 2004.
- 628 Strzepek, R. F., Hunter, K. A., Frew, R. D., Harrison, P. J. and Boyd, P. W.: Iron-light  
629 interactions differ in Southern Ocean phytoplankton, *Limnol. Oceanogr.*, 57(4), 1182–1200,  
630 doi:10.4319/lo.2012.57.4.1182, 2012.
- 631 Strzepek, R. F., Maldonado, M. T., Higgins, J. L., Hall, J., Safi, K., Wilhelm, S. W. and Boyd,  
632 P. W.: Spinning the “Ferrous Wheel”: The importance of the microbial community in an iron  
633 budget during the FeCycle experiment, *Global Biogeochem. Cycles*, 19(4), 1–14,  
634 doi:10.1029/2005GB002490, 2005.

- 635 Sunda, W. G. and Huntsman, S. A.: Iron uptake and growth limitation in oceanic and coastal  
636 phytoplankton, *Mar. Chem.*, 50(1-4), 189–206, doi:10.1016/0304-4203(95)00035-P, 1995.
- 637 Sunda, W. G. and Huntsman, S. A.: Interrelated influence of iron, light and cell size on  
638 marine phytoplankton growth, *Nature*, 390, 389–392, doi:10.1038/37093, 1997.
- 639 Tang, D. and Morel, F. M. M.: Distinguishing between cellular and Fe-oxide-associated trace  
640 elements in phytoplankton, *Mar. Chem.*, 98(1), 18–30, doi:10.1016/j.marchem.2005.06.003,  
641 2006.
- 642 Tortell, P. D., Maldonado, M. T. and Price, N. M.: The role of heterotrophic bacteria in iron-  
643 limited ocean ecosystems, *Nature*, 383(6598), 330–332, doi:10.1038/383330a0, 1996.
- 644 Toulza, E., Tagliabue, A., Blain, S. and Piganeau, G.: Analysis of the global ocean sampling  
645 (GOS) project for trends in iron uptake by surface ocean microbes., edited by F. Rodriguez-  
646 Valera, *PLoS One*, 7(2), e30931, doi:10.1371/journal.pone.0030931, 2012.

647

648 **Table 1** Location, date, depth of sampling and main biogeochemical properties from studied stations. Experimental approach column refers to  
 649 Figure 1 with a, b and c related to incubations including the whole community, pico-nanoplankton plus bacteria, and bacteria only, respectively.

Station	Latitude S	Longitude E	Date of sampling (dd/mm/yyyy)	Depth of sampling (m)	SST (°C)	NO <sub>3</sub> <sup>-</sup> + NO <sub>2</sub> <sup>-*</sup> (μmol L <sup>-1</sup> )	PO <sub>4</sub> <sup>3-*</sup> (μmol L <sup>-1</sup> )	Si(OH) <sub>4</sub> <sup>§</sup> (μmol L <sup>-1</sup> )	Chla <sup>∞</sup> (μg L <sup>-1</sup> )	DFe <sup>†</sup> (nmol L <sup>-1</sup> )	Experimental approach ‡
<b>HNLC reference</b>											
R-2	-50.3590	66.7170	26/10/2011	40	2.3	25.4	1.81	12.1	0.32	0.09	b, c
<b>Kerguelen plateau</b>											
A3-2	-50.6240	72.0560	17/11/2011	20	2.3	25.2	1.75	18.4	1.6	0.18	a, b, c
<b>Polar Front</b>											
F-L	-48.5320	74.6590	07/11/2011	20	4.3	18.5	0.900	6.45	2.8	0.26	b
<b>Downstream plume</b>											
E-2	-48.5230	72.0770	01/11/2011	20	3.0	26.6	1.74	14.5	0.42	0.08	b
E-3	-48.7020	71.9670	02/11/2011	20	3.1	25.4	1.78	15.1	0.079	0.38	b
E-4W	-48.7650	71.4250	12/11/2011	20	2.7	25.3	1.74	17.5	0.56	0.20	b, c
E-4E	-48.7150	72.5630	13/11/2011	20	3.2	24.3	1.62	12.1	1.3	0.19	a, b, c
E-5	-48.4120	71.9000	19/11/2011	20	3.3	25.0	1.73	11.5	1.1	0.06	a, b, c

650

651 \* From Blain et al., 2014

652 § From Closset et al., 2014

653 ∞ From Lasbleiz et al., 2014

654 † From Qu erou e et al., 2015

655 ‡ see for details Figure 2 and section 2.3

656 **Table 2**

657 List of abbreviations used.

Symbols	Explanation
$\rho Fe$	Total iron uptake
$\rho Fe_{bact}^{alone}$	Bacterial iron uptake determined in incubations with bacterial cells alone (size-fraction < 0.8 $\mu$ m, Fig. 2c)
$\rho Fe_{bact}^{<25\mu m}$	Bacterial iron uptake determined in incubations with pico- and nanoplankton only (size-fraction < 25 $\mu$ m, Fig. 2b)
$\rho Fe_{bact}^{whole}$	Bacterial iron uptake determined in incubations with the whole community (unfiltered seawater, Fig. 2a)
$\rho Fe: POC$	Total iron uptake normalized to particulate organic carbon
$(\rho Fe: POC)_{bact}^{alone}$	Bacterial iron uptake determined in incubations with bacterial cells alone (size-fraction < 0.8 $\mu$ m, Fig. 2c) normalized to particulate organic carbon
$(\rho Fe: POC)_{bact}^{<25\mu m}$	Bacterial iron uptake determined in incubations with pico- and nanoplankton only (size-fraction < 25 $\mu$ m, Fig. 2b), normalized to particulate organic carbon
$(\rho Fe: POC)_{bact}^{whole}$	Bacterial iron uptake determined in incubations with the whole community (unfiltered seawater, Fig. 2a) normalized to particulate organic carbon

658

659 **Table 3** Iron uptake rates ( $\rho\text{Fe}$ ), carbon biomass (POC), and C-normalized Fe uptake rates ( $\rho\text{Fe:POC}$ ) of the bulk community and the three size-  
660 fractions for incubations conducted at 75, 25 and 1% of the photosynthetically active radiation (PAR, % of surface PAR) on unfiltered seawater  
661 (see text and Figure 2a for details).

	Fe uptake rate ( $\text{pmol Fe L}^{-1} \text{d}^{-1}$ )				C biomass ( $\mu\text{mol C L}^{-1}$ )			C-normalized Fe uptake rate ( $\mu\text{mol Fe d}^{-1} \text{mol C}^{-1}$ )		
	PAR	A3-2	E-4E	E-5	A3-2	E-4E	E-5	A3-2	E-4E	E-5
Bulk community (>0.2 $\mu\text{m}$ )*	75	33.2	28.1	39.5	10.2	10.1	6.2	3.26	2.78	6.33
	25	19.0	26.5	32.7	10.2	10.4	6.2	1.86	2.56	5.27
	1	39.8	22.6	26.3	10.3	11.1	6.2	3.87	2.03	4.23
Microplankton (>25 $\mu\text{m}$ )	75	15.5	13.4	33.7	6.9	5.4	2.9	2.25	2.50	11.56
	25	5.1	13.2	22.4	6.8	5.3	2.9	0.75	2.47	7.68
	1	17.9	13.5	15.3	6.9	5.4	2.9	2.60	2.52	5.25
Pico-nanoplankton (0.8-25 $\mu\text{m}$ )	75	17.7	14.3	5.3	3.0	12.0	2.7	5.84	1.19	1.93
	25	13.3	12.8	9.9	3.0	12.0	2.7	4.39	1.07	3.61
	1	21.3	8.8	10.1	3.0	12.1	2.8	7.03	0.73	0.39
Heterotrophic bacteria (0.2-08 $\mu\text{m}$ )	75	0.07	0.30	0.46	0.3	0.7	0.6	0.21	0.45	0.80
	25	0.60	0.43	0.41	0.4	0.8	0.6	1.69	0.52	0.73
	1	0.57	0.34	0.39	0.4	0.7	0.6	1.37	0.49	0.66

662 \*  $\rho\text{Fe:POC}$  for bulk community was calculated as the sum of the iron uptake rates of the three size-fractions divided by the sum of particulate organic carbon of each size-  
663 fraction.  
664

665 **Table 4** Euphotic layer integrated Fe uptake of the bulk community and three size-fractions.  
 666 The depth of the euphotic layer is 39m for A3-2, 80m for E-4E and 41m for E-5.

<b>Station</b>	<b>Euphotic layer integrated Fe uptake (<math>\mu\text{mol Fe m}^{-2} \text{d}^{-1}</math>)</b>			
	Bulk community ( $>0.2 \mu\text{m}$ )	Microplankton ( $> 25\mu\text{m}$ )	Pico-nanoplankton ( $0.8-25\mu\text{m}$ )	Heterotrophic bacteria ( $0.2-0.8\mu\text{m}$ )
A3-2	1.12	0.44	0.66	0.019
E-4E	0.86	0.45	0.40	0.013
E-5	1.74	1.21	0.51	0.023

**Table 5** Bacterial carbon biomass, bacterial Fe uptake rates, C-normalized Fe uptake rates, and integrated Fe uptake (to the euphotic layer depth, Ze; to the mixed layer depth, MLD; average, avg). Values given in the columns  $(POC)_{bact}^{<25\mu m}$ ,  $(\rho Fe)_{bact}^{<25\mu m}$ , and  $(\rho Fe: POC)_{bact}^{<25\mu m}$  are relative to incubations with pico-nanoplankton only. Values given in the columns  $(POC)_{bact}^{whole}$ ,  $(\rho Fe)_{bact}^{whole}$ , and  $(\rho Fe: POC)_{bact}^{whole}$  are relative to incubations performed with the bulk community. Integrated values are calculated from incubations in absence of microplankton. *n.d.*: no data available. Cell numbers refer to the end of the incubation time (24 h).

Station	PAR level	Cell abundance ( $\times 10^5$ cells mL <sup>-1</sup> )		Biomass ( $\mu$ g C L <sup>-1</sup> )		Fe uptake rate (pmol Fe L <sup>-1</sup> d <sup>-1</sup> )		C-normalized Fe uptake rate ( $\mu$ mol Fe d <sup>-1</sup> mol C <sup>-1</sup> )		Integrated Fe (nmol Fe m <sup>-2</sup> d <sup>-1</sup> )		
		$(POC)_{bact}^{<25\mu m}$	$(POC)_{bact}^{whole}$	$(POC)_{bact}^{<25\mu m}$	$(POC)_{bact}^{whole}$	$(\rho Fe)_{bact}^{<25\mu m}$	$(\rho Fe)_{bact}^{whole}$	$(\rho Fe: POC)_{bact}^{<25\mu m}$	$(\rho Fe: POC)_{bact}^{whole}$	Ze	MLD	avg
E-4E	75%	10.82	6.49	13.42	8.05	0.10	0.30	0.09	0.45			
	45%	6.74	<i>n.d.</i>	8.36	<i>n.d.</i>	0.19	<i>n.d.</i>	0.28	<i>n.d.</i>			
	25%	5.89	7.95	7.30	9.86	0.16	0.43	0.26	0.52			
	16%	6.89	<i>n.d.</i>	8.54	<i>n.d.</i>	0.40	<i>n.d.</i>	0.56	<i>n.d.</i>	<b>9.7</b>	<b>12.8</b>	<b>11.3</b>
	4%	7.80	<i>n.d.</i>	9.67	<i>n.d.</i>	0.23	<i>n.d.</i>	0.28	<i>n.d.</i>			
	1%	7.07	6.73	8.77	8.35	0.17	0.34	0.23	0.49			
A3-2	75%	<i>n.d.</i>	3.50	<i>n.d.</i>	4.34	0.25	0.07	<i>n.d.</i>	0.21			
	45%	3.52	<i>n.d.</i>	4.36	<i>n.d.</i>	0.19	<i>n.d.</i>	0.51	<i>n.d.</i>			
	25%	3.75	3.45	4.65	4.28	0.10	0.60	0.26	1.69			
	16%	3.60	<i>n.d.</i>	4.46	<i>n.d.</i>	0.11	<i>n.d.</i>	0.30	<i>n.d.</i>	<b>6.6</b>	<b>13.1</b>	<b>9.9</b>
	4%	6.39	<i>n.d.</i>	7.92	<i>n.d.</i>	0.18	<i>n.d.</i>	0.27	<i>n.d.</i>			
	1%	3.78	4.01	4.69	4.97	0.16	0.57	0.40	1.37			
E-5	75%	5.29	5.59	6.56	6.93	0.05	0.46	0.10	0.80			
	45%	5.55	<i>n.d.</i>	6.88	<i>n.d.</i>	0.06	<i>n.d.</i>	0.10	<i>n.d.</i>			
	25%	5.18	5.39	6.42	6.68	0.07	0.41	0.13	0.73			
	16%	5.45	<i>n.d.</i>	6.76	<i>n.d.</i>	0.06	<i>n.d.</i>	0.11	<i>n.d.</i>	<b>5.2</b>	<b>4.2</b>	<b>4.7</b>
	4%	6.66	<i>n.d.</i>	8.26	<i>n.d.</i>	0.13	<i>n.d.</i>	0.19	<i>n.d.</i>			
	1%	5.18	5.74	6.42	7.12	0.14	0.39	0.27	0.66			
R-2	75%	2.84		3.52		0.07		0.23				
	45%	2.55		3.16		0.04		0.14				
	25%	<i>n.d.</i>		<i>n.d.</i>	<i>n.d.</i>	0.00		<i>n.d.</i>				
	16%	2.90	<i>n.d.</i>	3.60	<i>n.d.</i>	0.25	<i>n.d.</i>	0.82	<i>n.d.</i>	<b>4.4</b>	<b>5.0</b>	<b>4.7</b>
	4%	2.85		3.53		0.05		0.16				
	1%	2.65		3.29		0.05		0.19				

E-2	75%	4.30		5.33		0.07		0.16				
	45%	4.84		6.00		0.05		0.09				
	25%	5.48	<i>n.d</i>	6.80	<i>n.d</i>	0.06	<i>n.d</i>	0.11	<i>n.d</i>	<b>5.8</b>	<b>5.8</b>	<b>5.8</b>
	16%	<i>n.d</i>		n.d		0.27		n.d				
	4%	5.68		7.04		0.05		0.09				
	1%	5.32		6.60		<i>n.d</i>		0.06				
E-3	75%	6.98		8.66		15.50		21.4				
	45%	5.83		7.23		0.25		0.41				
	25%	7.85	<i>n.d</i>	9.73	<i>n.d</i>	0.41	<i>n.d</i>	0.51	<i>n.d</i>	<b>20.0*</b>	<b>16.8*</b>	<b>18.4*</b>
	16%	6.96		8.63		0.25		0.35				
	4%	8.49		10.53		0.32		0.36				
	1%	7.27		9.01		0.29		0.39				
F-L	75%	5.23		6.49		0.84		1.56				
	45%	7.80		9.67		0.36		0.45				
	25%	7.80	<i>n.d</i>	9.67	<i>n.d</i>	0.58	<i>n.d</i>	0.72	<i>n.d</i>	<b>14.0</b>	<b>18.4</b>	<b>16.2</b>
	16%	0.82		1.02		0.25		2.94				
	4%	3.82		4.74		0.50		1.26				
	1%	22.36		27.73		0.49		0.21				
E-4W	75%	6.63		8.22		0.17		0.25				
	45%	6.70		8.31		0.21		0.30				
	25%	5.07	<i>n.d</i>	6.29	<i>n.d</i>	0.71	<i>n.d</i>	1.36	<i>n.d</i>	<b>13.8</b>	<b>16.6</b>	<b>15.2</b>
	16%	19.40		24.06		0.23		0.11				
	4%	13.90		17.24		0.21		0.15				
	1%	7.75		9.61		0.29		0.35				

\* Integrated value measured at 75% was excluded of the calculation.

**Table 6** Carbon normalized Fe uptake rates for bacteria and pico-nanoplankton. Columns  $(\rho\text{Fe:POC})_{\text{bact}}^{<25\mu\text{m}}$  and  $(\rho\text{Fe:POC})_{\text{bact}}^{\text{alone}}$  are for bacteria incubated with pico-nanoplankton only and bacteria incubated alone, respectively. The column  $(\rho\text{Fe:POC})_{\text{pico-nano}}$  stands for pico-nanoplankton. We note that this Fe uptake rate was measured during incubations with bacteria. Because pico-nanoplankton largely outcompeted bacteria, this rate is a good approximation of the Fe uptake rate for pico-nanoplankton incubated alone. Values are from incubations performed at 1% of the PAR level.

$\rho\text{Fe:POC}$ ( $\mu\text{mol Fe d}^{-1} \text{mol C}^{-1}$ )			
Station	$(\rho\text{Fe:POC})_{\text{bact}}^{<25\mu\text{m}}$	$(\rho\text{Fe:POC})_{\text{pico-nano}}$	$(\rho\text{Fe:POC})_{\text{bact}}^{\text{alone}}$
A3-2	0.40	7.04	5.17
E4-E	0.23	0.73	1.54
E-5	0.27	3.88	1.43
E4-W	0.35	4.13	9.13
R2	0.19	0.14	0.24

Figure 1

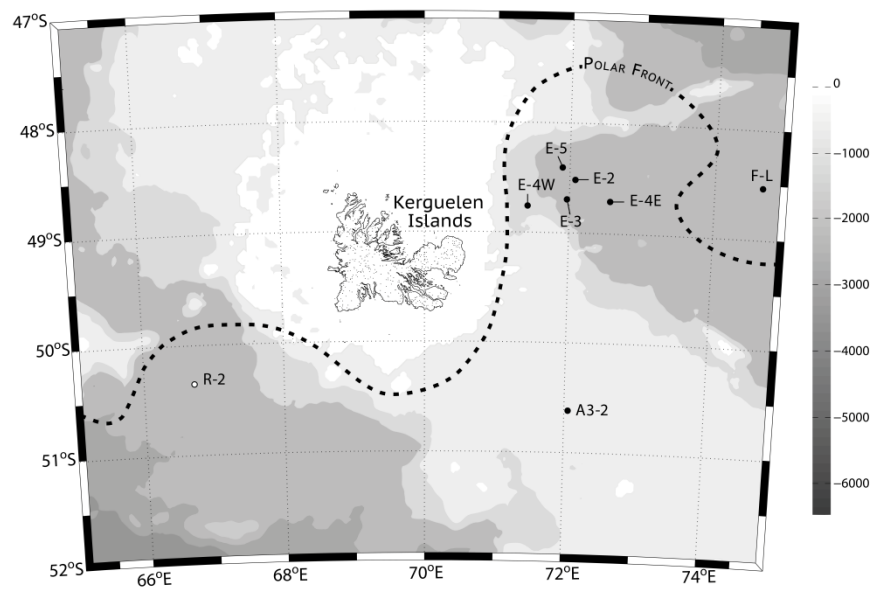


Figure 2

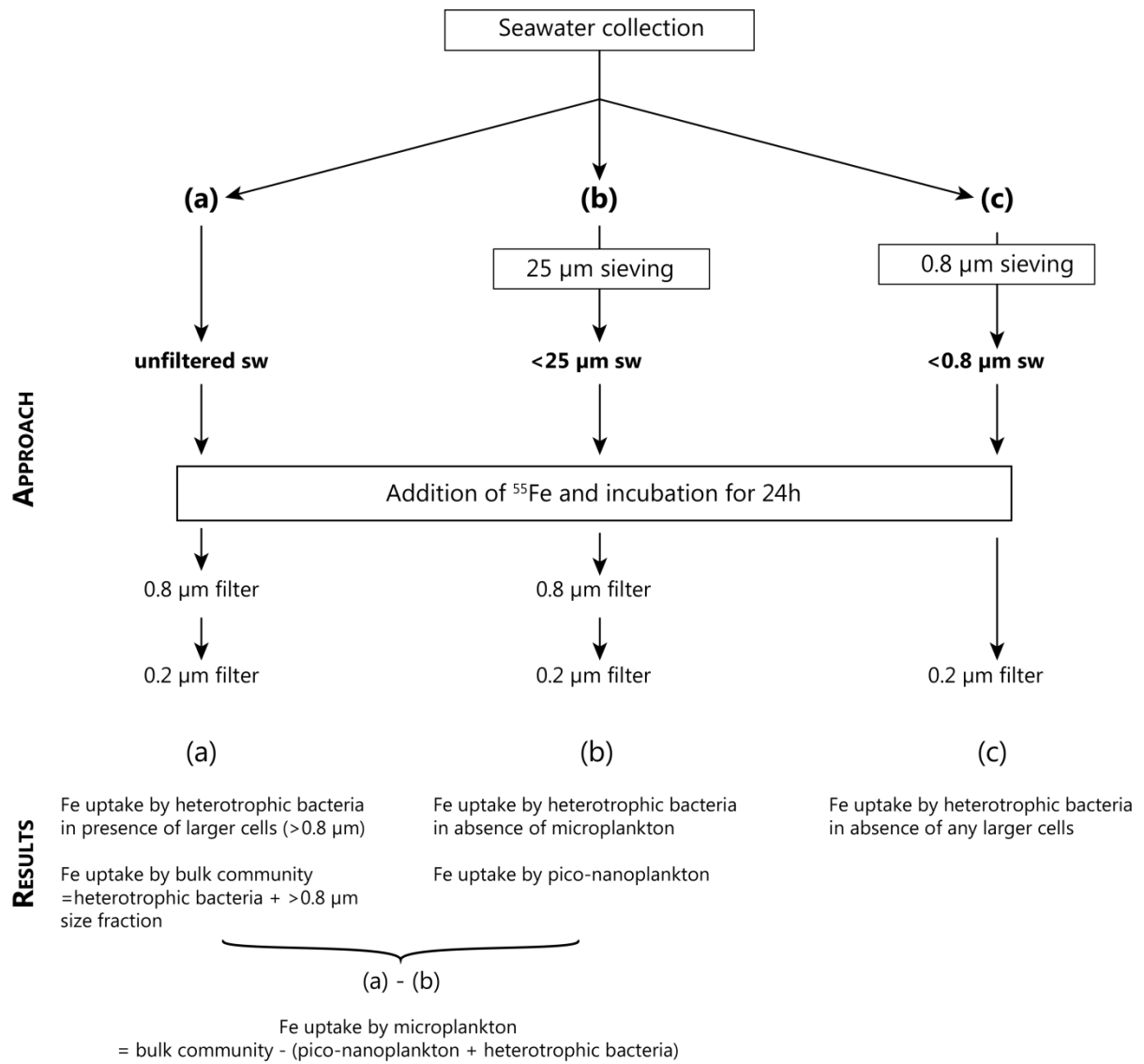


Figure 3

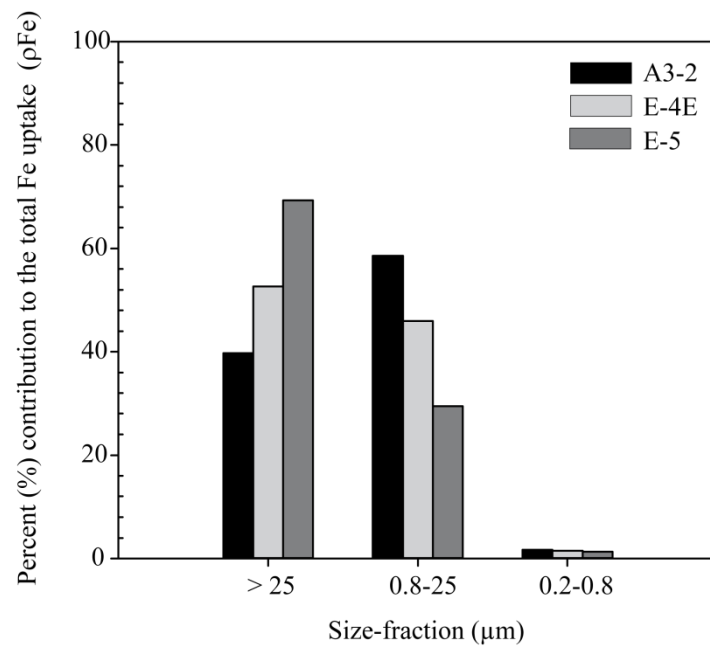


Figure 4

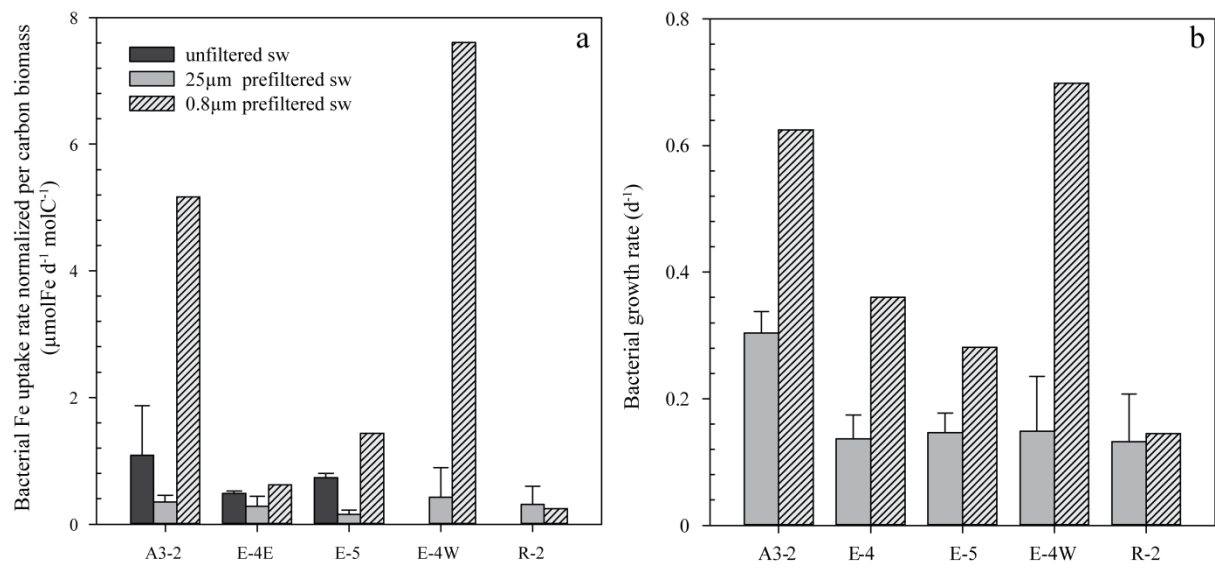


Figure 5

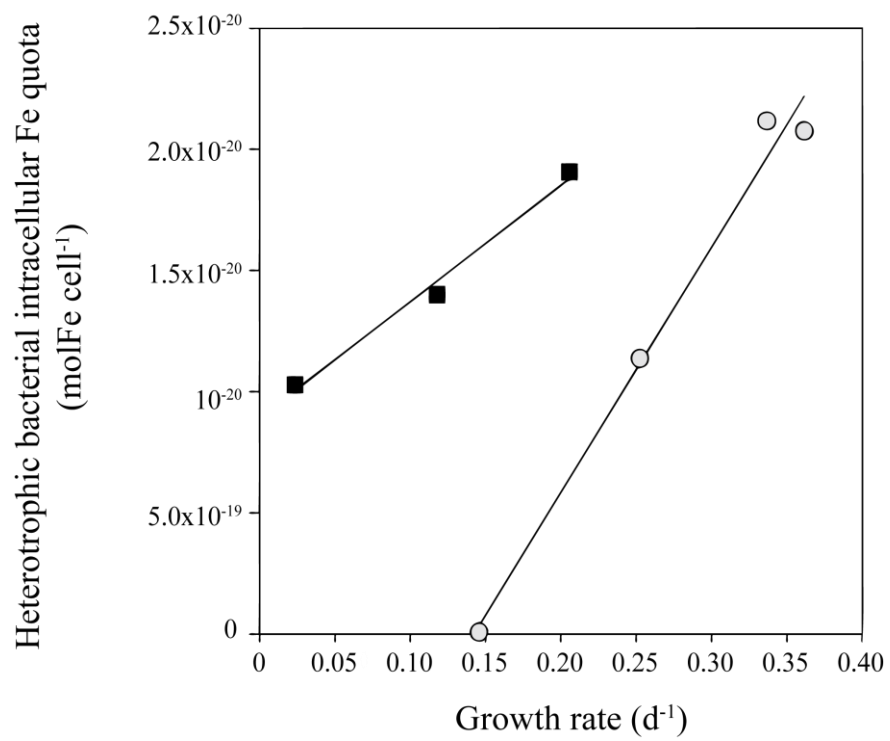


Figure 6

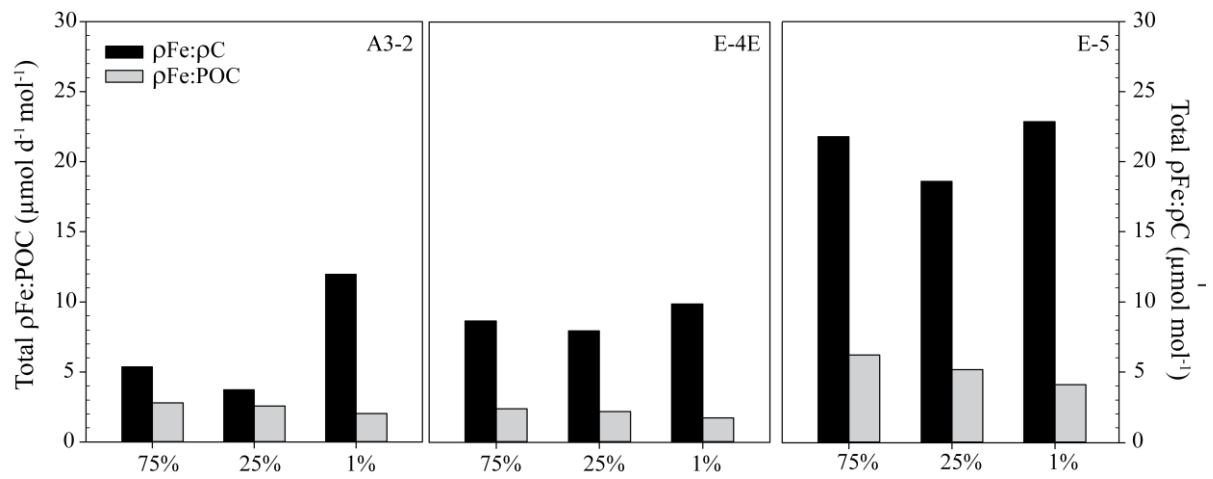


Figure 7

